

Article

Iterative Investigation of Wind Environments Influenced by Bulge-Part Geometries of Typical T-Form High-Rise Buildings Using Parametric Modelling, CFD and IAs Analysis

Han Guo^{1,2}, Yawen Liu³  and Yi He^{2,*} 

¹ Key Laboratory of Urban Land Resources Monitoring and Simulation, Ministry of Natural Resources of China, Shenzhen 518040, China; guohan@whu.edu.cn

² School of Architecture and Urban Planning, Huazhong University of Science and Technology, Wuhan 430074, China

³ School of Computer Science, Hubei University of Technology, Wuhan 430068, China; liuyawen_prs@whu.edu.cn

* Correspondence: yihe@hust.edu.cn

Abstract: Although T-form buildings have been widely observed in newly constructed high-rise residential communities, there have been relatively limited investigations into the influence of their geometries on wind environments. This study aims to address this gap by conducting iterative quantitative assessments of the influences of various bulge-part sizes of typical T-form high-rise residential buildings on surrounding wind environments. A methodology has been employed by integrating multiple computational tools, including parametric modeling, Computational Fluid Dynamics (CFD), and Influenced Areas (IAs) analysis. Representative T-form buildings have been modeled with parametric components, allowing for easy variation of bulge-part sizes. The investigation process involves sequential steps of parametric modeling, experimentally validated CFD simulations, statistical assessment, and subsequent results analysis and discussions. Findings could be summarized as follows: (1) according to IAs analysis, the influences on wind environments were decreased as the bulge-part sizes were increased, and the decrease of the bulge-part sizes could cause the contrary effect; (2) the promotion of outdoor ventilation caused by the increase of the bulge-part length was more than the increase of the bulge-part width according to the correlation coefficients ($0.88 > 0.78$; $0.88 > 0.76$); (3) it was recommended to design relatively large bulge parts on the windward side to enhance outdoor ventilation. The research outcomes provide valuable and insightful information for the development of sustainable architectural design strategies aimed at optimizing natural ventilation.

Keywords: iterative quantitative investigation; wind environments; T-form; high-rise building; multiple computational tools



Citation: Guo, H.; Liu, Y.; He, Y. Iterative Investigation of Wind Environments Influenced by Bulge-Part Geometries of Typical T-Form High-Rise Buildings Using Parametric Modelling, CFD and IAs Analysis. *Sustainability* **2024**, *16*, 3354. <https://doi.org/10.3390/su16083354>

Academic Editor: Antonio Caggiano

Received: 11 February 2024

Revised: 15 March 2024

Accepted: 28 March 2024

Published: 17 April 2024



Copyright: © 2024 by the authors. Licensee MDPI, Basel, Switzerland. This article is an open access article distributed under the terms and conditions of the Creative Commons Attribution (CC BY) license (<https://creativecommons.org/licenses/by/4.0/>).

1. Introduction

In contemporary discourse, research on wind environments has gained significant traction due to its intrinsic connection to the development of sustainable habitats [1]. Among the myriad factors influencing sustainable living, natural ventilation in residential buildings stands out as paramount, impacting both energy conservation and the well-being of occupants [2]. In response to burgeoning urban populations, particularly in developing regions, metropolitan areas have witnessed a surge in the construction of residential buildings characterized by innovative forms and configurations [3,4]. This trend underscores the pressing need for a deeper understanding of how these architectural innovations influence wind dynamics and, by extension, the livability and sustainability of urban environments.

1.1. Outdoor Wind Environments around Buildings

The understanding of outdoor wind environments around buildings has historically been overshadowed in architectural discourse, with more emphasis placed on indoor comfort rather than broader environmental considerations. However, a seminal review by Blocken et al. underscored the crucial significance of integrating building design with outdoor wind dynamics, advocating for a shift towards a comprehensive understanding of wind environments beyond building envelopes [5]. This review illuminated the multifaceted effects, comforts, hazards, and climatic implications of wind patterns, particularly highlighting typical flow patterns around buildings and their implications at the pedestrian level. Over the past two decades, numerous studies have deepened our understanding of wind environments at the pedestrian level, recognizing wind speed as a pivotal parameter influencing outdoor human comfort in urban settings. For instance, Stathopoulos proposed an integrated index incorporating wind speed, temperature, and relative humidity to evaluate urban environmental conditions comprehensively [6].

The impact of buildings on wind dynamics primarily stems from their forms and configurations. Architectural elements such as shape, size, orientation, and arrangement significantly influence wind flow, leading to obstruction or acceleration [7,8]. Studies by Tsang et al. conducted comprehensive parametric wind tunnel studies elucidating wind-structure interactions and their implications on pedestrian-level wind environments, considering factors like building dimensions, separations, and arrangements under different wind conditions [9]. Similarly, Luo et al. explored complex flow patterns behind cuboid obstacles, revealing intricate relationships between flow incidence angles, obstacle shapes, and wind tunnel experimental models [10]. Moreover, research has demonstrated the influence of building height and width on wind comfort and natural ventilation. Du et al. highlighted the potential of increased building height to enhance wind comfort within building boundaries [11], while Tsang et al. cautioned against the adverse effects of widening buildings on natural ventilation [9]. Zhou et al. showcased the efficacy of design optimization in reducing air age through strategic adjustments in building orientation, spacing, creation of wind paths, and window configurations, employing Computational Fluid Dynamics (CFD) modeling techniques [3]. These findings underscore the intricate interplay between architectural design choices and outdoor wind environments, offering valuable insights for the development of sustainable urban environments. Jiang et al. conducted a study to offer novel insights into optimizing the wind environment within enclosed courtyards by quantitatively analyzing the effects of opening position, size, and wind angle using computational fluid dynamics (CFD) simulations, establishing comfort wind zone ratio (CWZR) models for different scenarios, thereby providing valuable guidance for courtyard building design and enhancing outdoor comfort in urban spaces [12].

Jie et al. provided a comprehensive review of the impact mechanisms of urban wind environments on urban building energy consumption, addressing a gap in the existing literature by examining building-scale and city-scale simulation tools and proposing future directions to enhance accuracy and validation methods in energy consumption calculations considering urban wind environments [13]. Oh et al. developed a novel approach utilizing building-resolved large-eddy simulation (LES) to analyze the thermal wind environment in urban areas with high-rise buildings, incorporating seasonal atmospheric data and validating the method against wind tunnel experiments, showcasing the occurrence of downdraft winds and large-circulation induced by high-rise buildings, which significantly influence pedestrian-level temperatures and urban thermal environments [14]. Ying et al. introduced an innovative approach to address the conflict between building density and external environmental comfort in high-density residential layouts, particularly in Chinese cities, by proposing an intelligent planning method that combines genetic algorithms and convolutional neural networks to automatically generate optimized layouts while efficiently simulating wind environments, offering a practical solution to enhance urban living conditions [15]. Chen et al. utilized large eddy simulations to investigate the pedestrian-level wind environment around elevated walkways in ideal urban street

canyons, elucidating the influence of street aspect ratio, walkway width, and sidewall type on mean and gust wind velocities. The findings highlighted the adverse effects of elevated walkways on pedestrian wind conditions and provided insights into optimal design considerations for enhancing pedestrian comfort and safety in urban environments [16]. Liu et al. evaluated the performance of Steady Reynolds Averaged Navier–Stokes (SRANS), Large Eddy Simulation (LES), and Detached Eddy Simulation (DES) models in predicting wind flow around an isolated high-rise building, with particular emphasis on the effectiveness of the Delayed Detached Eddy Simulation (DDES) model in capturing both mean flow fields and instantaneous wind characteristics, offering potential for enhanced accuracy in outdoor wind and thermal comfort analysis [17].

1.2. Review of T-Form Buildings

A building unit is typically characterized by an independent entrance and a vertical traffic system [18]. Within this context, the term “T-form” refers to a building unit with an architectural configuration resembling the shape of the capital letter “T” (Figure 1). This configuration is derived from the conventional rectangular form by introducing a bulging midsection on one side, often utilized as balconies, particularly common in residential structures with fewer floors, typically less than 12. With the demand for larger apartments and the proliferation of taller buildings, these bulge parts have grown in size. A typical floor plan of a relatively tall T-form building includes four apartments, typically with two apartments situated within the bulge part. This layout optimizes space efficiency, with a central transportation core positioned on the north side and an aisle separating the elevator shaft and staircase. In the event of a fire, the aisle facilitates smoke exhaust through the staircase without the need for a mechanical ventilation system. The primary advantages of T-form buildings lie in their ability to accommodate larger apartments while efficiently utilizing land space, all the while providing sensible orientations for most apartments. T-form buildings offer versatility in size adjustment, catering to the preferences of both developers and clients, hence their popularity in urban areas today. However, these buildings also present drawbacks, such as limitations in seasonal wind circulation through the bulge-part apartments in the south-north direction, attributable to the absence of window openings on the north side due to the presence of the aisle and transportation core. Additionally, the bulge parts may occasionally overshadow other areas of the T-form buildings, particularly those with larger dimensions. In summary, T-form buildings represent a logical and popular architectural choice in the urban landscapes of developing regions [18]. Modifications of the T-form concept, such as irregular forms, have also been explored.



Figure 1. (Left) and (Middle): Typical examples of high-rise residential T-form buildings. (Right): An example of the simplified floor plan of ‘T’ form.

Despite their prevalence, there is a paucity of research on T-form buildings. For instance, Iqbal et al. examined the impact of wind incident angles and passage widths on wind flow characteristics at the re-entrant corners of cross-shaped high-rise buildings [19]. These cross-shaped buildings share similarities with T-form structures due to the presence of bulge parts in the middle. The study revealed that building orientations and separations significantly influenced wind circulation at re-entrant corners, with oblique wind directions leading to the formation of unstable vortices, impacting contaminant dispersion and wind

comfort. The wind catchment effect and sheltering effect were also explored within this context [13].

1.3. Summary

(1) Research gaps

Previous studies have primarily focused on analyzing wind environments around conventional building forms like cuboids, with limited attention paid to irregular structures such as T-form buildings. Consequently, our understanding of wind environment characteristics specific to T-form buildings and the effects of building variables has remained rudimentary. Given the increasing prevalence of T-form buildings in recent years, there is a critical need to investigate their wind environments to extract insights essential for developing sustainable design strategies and optimizing microclimates.

(2) Research framework

This study aims to conduct a quantitative analysis of the influences exerted on pedestrian-level wind environments by contemporary high-rise residential T-form buildings. It seeks to elucidate the relationships between these influences and various bulge-part sizes, encompassing both width and length variations. Specifically, the investigation examines two distinct types of buildings: a series of shorter structures with a height of 36 m and another series of taller edifices towering at 72 m. The Optic Valley Area in Wuhan City was selected as the study site due to its representativeness for developing regions. Influences are defined in terms of the areas affected by different wind velocity magnitudes on a horizontal plane at the 1.5 m pedestrian level surrounding buildings. Key parameters under scrutiny include Influence Areas (IAs) corresponding to various wind velocities, Low-Velocity Areas (LVAs) on leeward sides, and High-Velocity Areas (HVAs) along lateral sides. A comprehensive methodology integrating multiple computational tools is deployed for quantitative analysis of these influences on wind environments. The study examines and compares 14 cases of T-form buildings, divided into two parts. Results analysis encompasses the evaluation of IAs, LVAs, HVAs, air-pressure magnitudes, and wind flow streamlines, collectively shedding light on the distinctive wind environment characteristics surrounding T-form buildings across a spectrum of bulge-part sizes.

2. Methodology

A comprehensive methodology was meticulously crafted, encompassing geometric analysis, parametric modeling, Computational Fluid Dynamics (CFD) simulations, and influence analysis. Commencing with an exhaustive exploration of the geometric attributes of T-form high-rise residential buildings within a developing locale, a selection of representative building cases showcasing diverse bulge-part sizes was identified for detailed investigation. Subsequently, a sophisticated parametric modeling system was established to streamline the creation of T-form building models with varying bulge-part configurations. Adhering rigorously to the esteemed Best Practice Guideline COST 732, CFD simulations were meticulously conducted in accordance with recognized industry standards [20]. Given the computationally demanding nature of the transient analysis, the Reynolds-Averaged Navier-Stokes (RANS) turbulence model was meticulously chosen for CFD simulations [19]. To ensure the utmost accuracy and reliability, a grid-independent analysis was rigorously performed, and the CFD method was meticulously validated through experimental verification. Quantitative evaluation of the influences on wind environments was conducted employing an image processing tool, thus furnishing a robust foundation for subsequent analysis and interpretation.

2.1. Building Geometries and Case Settings

The geometric investigation was conducted through comprehensive site surveys conducted in the Optic Valley Area of Wuhan City, focusing on residential structures that typify newly constructed buildings in burgeoning regions. Our analysis revealed

twelve distinct building typologies prevalent in the area. A statistical examination of urban architecture unveiled that T-form buildings constituted 73.11% of residential communities. This study delves into the impact of varying bulge-part dimensions on wind environments, particularly focusing on typical high-rise residential T-form buildings with two different heights (Part 1 and Part 2).

In Part 1, we scrutinized the effects of bulge parts with varying lengths on T-form buildings with a standard height of 36 m. These buildings, embodying 12 floors with two apartments per floor, represent relatively low-rise structures. We established five simulation cases with different bulge part lengths ranging from 6 m to 10 m while maintaining a fixed width of 2 m. The major part of the building consistently had a length of 20 m and a width of 10 m, as determined through our site investigations and geometric analyses.

Part 2 of our study investigates the influence of bulge parts with different widths and lengths on T-form buildings with a standard height of 72 m, representing taller structures comprising 24 floors with four apartments per floor. We designed nine simulation cases with bulge part lengths ranging from 15 m to 21 m and widths from 6 m to 18 m. The major part of these buildings maintained a consistent length of 39 m and a width of 12 m, based on our empirical data and geometric evaluations.

Detailed specifications for the five cases in Part 1 and nine cases in Part 2 are presented in the figures and tables below (Figure 2, Tables 1 and 2). Within the tables, “Length (M)” and “Width (M)” denote the dimensions of the major part of the building, while “Length (B)” and “Width (B)” represent those of the bulging part.

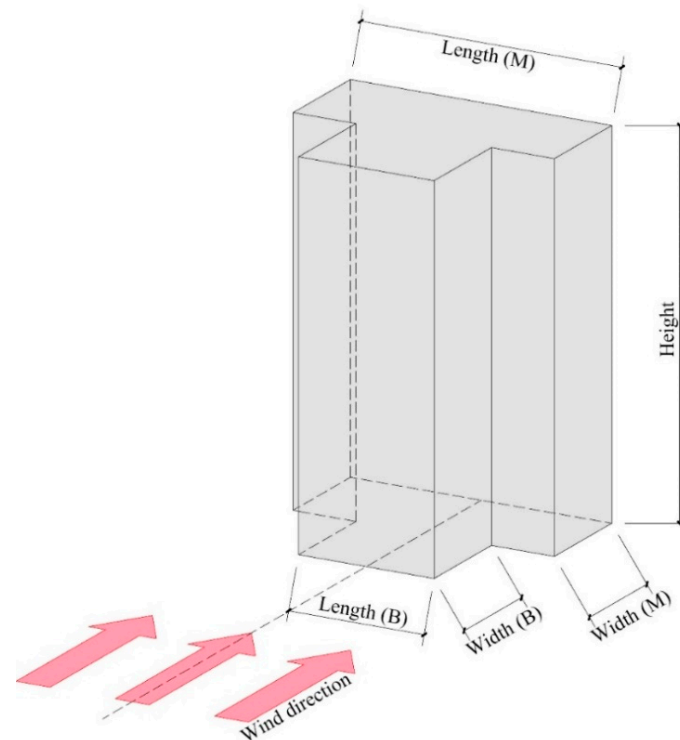


Figure 2. The architectural variables of T-form buildings.

Table 1. The five cases of Part 1.

Cases	Lengths (M)	Widths (M)	Heights	Lengths (B)	Widths (B)
Case 1	20 m	10 m	36 m	0 m	0 m
Case 2	20 m	10 m	36 m	6 m	2 m
Case 3	20 m	10 m	36 m	8 m	2 m
Case 4	20 m	12 m	36 m	0 m	0 m

Table 2. The nine cases of Part 2.

Cases	Lengths (M)	Widths (M)	Heights	Lengths (B)	Widths (B)
Case 1	39 m	12 m	72 m	15 m	6 m
Case 2	39 m	12 m	72 m	18 m	6 m
Case 3	39 m	12 m	72 m	21 m	6 m
Case 4	39 m	12 m	72 m	15 m	12 m
Case 5	39 m	12 m	72 m	18 m	12 m
Case 6	39 m	12 m	72 m	21 m	12 m
Case 7	39 m	12 m	72 m	15 m	18 m
Case 8	39 m	12 m	72 m	18 m	18 m
Case 9	39 m	12 m	72 m	21 m	18 m

2.2. Parametric Modelling of T-Form Buildings

We developed a parametric modeling script for T-form buildings using Grasshopper within Rhino, facilitating the creation of building models with ease. By inputting various parameters into the components, the parametric model becomes highly adaptable, enhancing modeling efficiency for iterative analysis across numerous cases [21]. Conceptually, a T-form building comprises a major part resembling a large cuboid and a bulge part resembling a smaller cuboid. While several modeling methods exist for creating T-form buildings, a straightforward approach involves assembling two rectangular cuboids. However, this method often leads to disjointed volumes at their contact surfaces, posing challenges for mesh generation and simulations.

To overcome this limitation, we adopted a modeling strategy that begins with defining the floor-plane surface and facades. The floor-plane surface is generated based on several reference points, with the height parameter determining the entire building's geometry. Specifically, eight points are utilized to define the floor-plane surface of a T-form building. Initially, four points delineate a rectangular surface representing the major part, while another four points define a smaller rectangular surface representing the bulge part. Each point requires three parameters ($\{x, y, z\}$ coordinates) for precise definition. Additionally, two sets of widths and lengths are designated to define the major and bulge parts, serving as the primary parameters for generating coordinates through scripts employing mathematical logic (refer to Figure 3). Consideration is also given to the positioning of these two parts during the modeling process. Ultimately, the 'Extrude' component is employed to construct the entire building model, with the height parameter determining its vertical extent.

2.3. Governing Equations

In this research, CFD simulations were conducted utilizing the RANS method. While alternative techniques such as Large Eddy Simulation (LES) and Direct Numerical Simulation (DNS) offer enhanced accuracy, they typically demand extensive computational resources and high-performance computing platforms [17,19,21]. Given the computational efficiency and sufficient accuracy demonstrated in prior studies [21,22], the RANS method was deemed suitable for the objectives of this study. Specifically, a k - ϵ model was adopted to close the Navier-Stokes (NS) equation system [23,24]. The transparent equations governing turbulent kinetic energy (k) and dissipation rate (ϵ) are presented below (Equations (1)–(5)).

$$\frac{\partial \rho k}{\partial t} + \frac{\partial \rho k u_i}{\partial x_i} = \frac{\partial}{\partial x_i} \left[\left(\mu + \frac{\mu_t}{\sigma_k} \right) \frac{\partial k}{\partial x_i} \right] + \frac{\partial u_i}{\partial x_j} \left(\mu_t s_{ij} - \frac{2}{3} \rho k \delta_{ij} \right) - \rho \epsilon + \mu_t P_B \quad (1)$$

$$\frac{\partial \rho \epsilon}{\partial t} + \frac{\partial \rho \epsilon u_i}{\partial x_i} = \frac{\partial}{\partial x_i} \left[\left(\mu + \frac{\mu_t}{\sigma_\epsilon} \right) \frac{\partial \epsilon}{\partial x_i} \right] + C_{\epsilon 1} \frac{\epsilon}{k} \left[f_1 \frac{\partial u_i}{\partial x_j} \left(\mu_t s_{ij} - \frac{2}{3} \rho k \delta_{ij} \right) + C_B \mu_t P_B \right] - f_2 C_{\epsilon 2} \frac{\rho \epsilon^2}{k} \quad (2)$$

$$s_{ij} = \frac{\partial u_i}{\partial x_j} + \frac{\partial u_i}{\partial x_i} - \frac{2}{3} \delta_{ij} \frac{\partial u_k}{\partial x_k} \quad (3)$$

$$P_B = -\frac{g_i}{\sigma_B} \frac{1}{\rho} \frac{\partial \rho}{\partial x_i} \quad (4)$$

$$\mu_t = f_u \frac{C_\mu \rho k^2}{\varepsilon} \quad (5)$$

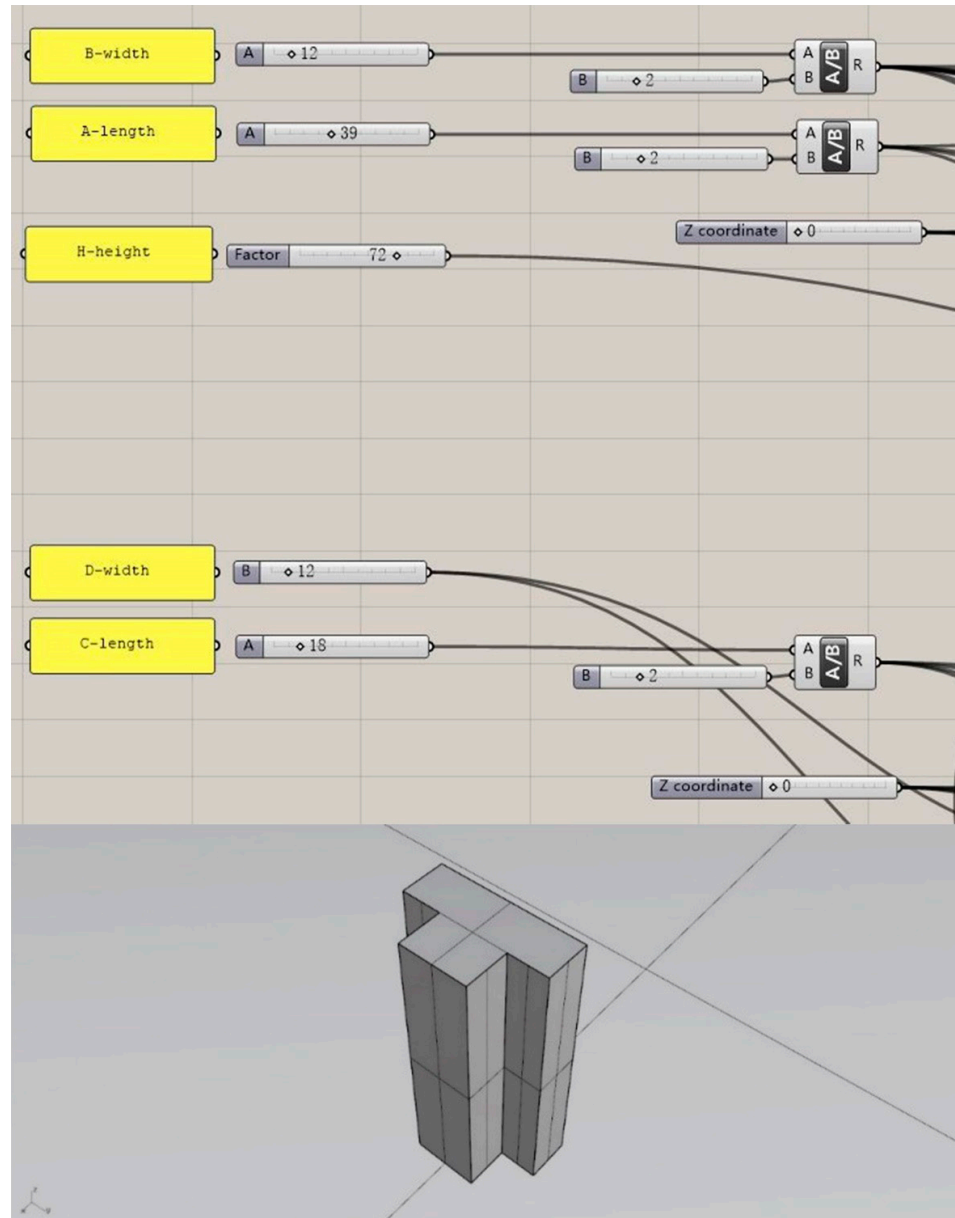


Figure 3. (Top): The parameters set in the parametric modeling of T-form buildings. (Bottom): A parametric model of T-form building.

In the presented equations, several parameters play key roles in governing the fluid dynamics. The symbol ρ represents the fluid density, while μ denotes the dynamic viscosity; the variable x_i was the coordinate of the unit volume, and u_i was the velocity of the unit volume x_j ; x_j was the coordinate of the unit volume, and u_j was the velocity of the unit volume x_k ; σ_k and σ_ε were two turbulence Prandtl numbers corresponding to the k and the ε [25]; C_μ , $C_{\varepsilon 1}$, and $C_{\varepsilon 2}$ were three empirical constants; μ_t was the turbulence viscosity [26]; the model reverted to the standard k - ε model if the damping functions of f_μ , f_1 and f_2 equaled

one [25]. $C_\mu = 0.09$, $C_{\epsilon 1} = 1.44$, $C_{\epsilon 2} = 1.92$; $\sigma_k = 1$, $\sigma_\epsilon = 1.3$, $\sigma_B = 0.9$; if $P_B > 0$, $C_B = 0$; if $P_B < 0$, $C_B = 1$ [25]. These parameters and their values significantly influence the behavior and outcomes of the fluid dynamics model.

2.4. Computational Domain and Boundary Condition

The wind conditions in our Computational Fluid Dynamics (CFD) simulations were determined using the locally recognized and widely utilized Chinese Standard Weather Data (CSWD). Through our calculations, we observed that the local wind velocity exhibited relative stability with minor fluctuations. Consequently, we adopted the annual average wind velocity of 1.33 m/s, measured at a height of 10 m, as our reference wind velocity for inlet calculations. The equations below presented the calculations of the wind velocity, turbulence kinetic energy, and turbulence dissipation ratio, respectively (Equations (6)–(8)) [27]. In the equations, z was the height, u_{ABL}^* was the ABL friction velocity which was set as the reference wind velocity, C_u was a turbulence model constant, z_0 was the aerodynamic roughness longitude which was set as 0.03 [28], κ was the von Karman constant which was set as 0.4. These parameters collectively provide a comprehensive framework for determining wind conditions and turbulence characteristics within our computational domain.

$$U(z) = \frac{u_{ABL}^*}{\kappa} \ln\left(\frac{z + z_0}{z_0}\right) \quad (6)$$

$$k(z) = \frac{u_{ABL}^{*2}}{\sqrt{C_u}} \quad (7)$$

$$\epsilon(z) = \frac{u_{ABL}^{*2}}{\kappa(z + z_0)} \quad (8)$$

The dimensions of our computational domain adhered to established guidelines outlined by the Committee on Operational Safety Trends (COST) for Computational Fluid Dynamics (CFD) simulations [20]. We structured the domain with a total length of 20H, where 5H represented the space ahead of the windward side of the buildings, and 15H comprised the area behind the leeward side. The building model was centrally positioned within the domain, occupying a width of 10H, equally distributed with 5H on each lateral side. Additionally, the domain's height was set at 7H. To ensure consistency in our comparisons of wind environments, all boundaries of the CFD simulation results were standardized in size.

In delineating the computational domain, we utilized cuboid cells generated through Cartesian-based technology. A body-fitted algorithm facilitated the subtraction of parametric building models during grid generation processes. Furthermore, to refine the grids, the cuboid cells were subdivided into eight smaller cuboids based on multiple adaptation criteria [24]. This meticulous approach to domain design and grid generation lays a robust foundation for accurate and insightful analyses of wind behavior and its effects on the built environment.

2.5. Grid-Dependence Analysis

For the grid-independent analysis, we constructed three sets of grids, namely the coarse grid consisting of 162,057 cells, the medium grid comprising 313,630 cells, and the fine grid totaling 618,521 cells [29]. These grids were tailored to a T-form building, with specific dimensions: a height of 72 m, major-part length of 39 m, major-part width of 12 m, bulge-part length of 18 m, and bulge-part width of 12 m. Utilizing the local Chinese Standard Weather Data (CSWD) for simulations, we evaluated velocity (V) and turbulent kinetic energy (TKE) at various heights along a vertical line situated at $x = 10$ m ahead of the centerline on the windward side of the T-form building. This systematic approach enables a comprehensive assessment of grid sensitivity, ensuring the reliability and accuracy of our computational results across different grid resolutions.

Our comparisons of the V and the TKE showed that the results of the three sets of grids had good agreements (Figure 4). The calculation of the grid convergence index (GCI) further confirmed the grid accuracy of the numerical method (Equation (9)) (Table 3) [30,31]. Because the calculation results of GCI, which were less than 5% could meet the suggestions given by several former studies [32]. The equation below presented the calculation of GCI:

$F_s = 1.25$ was the safety factor; $\varepsilon_{rms} = \left(\frac{\sum_{i=1}^{i=n} \varepsilon_i^2}{n} \right)^{\frac{1}{2}}$ was the root mean square relative error (in the equation, n was the number of measuring points); $r = 2$ was the grid refinement ratio; $p = 2$ was based on the discretization of all terms. The coarse grid set was adopted to ensure both the accuracy and efficiency of CFD simulations.

$$GCI = F_s \frac{\varepsilon_{rms}}{r^p - 1} \quad (9)$$

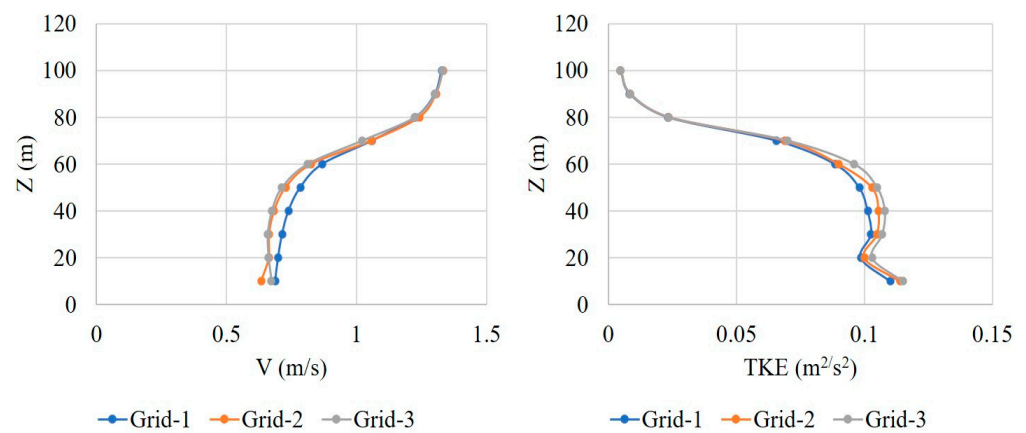


Figure 4. Comparisons of the velocity (V) and turbulent kinetic energy (TKE) of the three grid sets at $x = 10$ m in front of the building.

Table 3. GCI calculation of the wind velocity (V) and turbulent kinetic energy (TKE).

	Grids	Grid 1-2	Grid 2-3	Grid 1-3
V	ε_{rms} (%)	3.852	1.920	4.330
	GCI (%)	1.605	0.800	1.804
TKE	ε_{rms} (%)	0.278	0.247	0.479
	GCI (%)	0.116	0.103	0.200

2.6. CFD Simulation Validation Based on Experiment

The CFD simulation method was validated by a wind tunnel experiment of a published study of high-rise cross-shaped buildings conducted by researchers from the City University of Hong Kong [19]. The experiment was selected because the geometries of the high-rise cross-shaped buildings were similar to the T-form building for the bulge parts. As shown in Figure 5, we selected the ‘configuration-4 experiment’ of the study for validation. The buildings were modeled using the parametric method in Rhino’s GH. The building models could be adjusted efficiently for various simulations. All the parameters of the validation CFD simulation were set according to the wind tunnel experiment. The wind tunnel was 10.7 m long: the length before the leeward side of the buildings was 2.3 m, and the length behind the leeward side of the buildings was 8.4 m; the width of the wind tunnel was 2.5 m; the height of the wind tunnel was 2 m. For the inlet air-flow velocity, the reference wind velocity within the wind tunnel was set to 10 m/s at a height of 1.8 m, and the mean speed profile was fitted by a power law exponent of 0.15. The roughness length was set to 0.013 m. As shown in Figure 5, normalized wind speeds (NWSs) on the points of C1-C12 were

measured for the comparison of simulation and experiment. The speeds were normalized by using the reference wind speed at the height of 1.8 m. The comparisons showed that the results of normalized wind speeds were fitted quite well. The Predicted Root Mean Square Division (PRMSD), Normalized Mean Square Error (NMSE), and Fractional Bias (FB) were considered to evaluate statistical discrepancies between the simulation and experiment [33,34]. The calculation process was presented by the following equations (Equations (10)–(12)). As shown in the calculation results in Figure 6, the PRMSD, NMSE, and FB were all close to 0, $NMSE < 1.5$, and $-0.3 < FB < 0.3$. The results could meet the standards suggested by the COST criteria [35]. Therefore, the accuracy or reliability of the CFD simulation was demonstrated.

$$PRMSD_{ES} = \frac{1}{E_m} \times \sqrt{\sum_{i=1}^n \frac{(E_i - S_i)^2}{n}} \tag{10}$$

$$NMSE_{ES} = \frac{\sum_{i=1}^n (E_i - S_i)^2}{\sum_{i=1}^n (E_i \times S_i)} \tag{11}$$

$$FB_{ES} = \frac{E_m - S_m}{0.5 \times (E_m + S_m)} \tag{12}$$

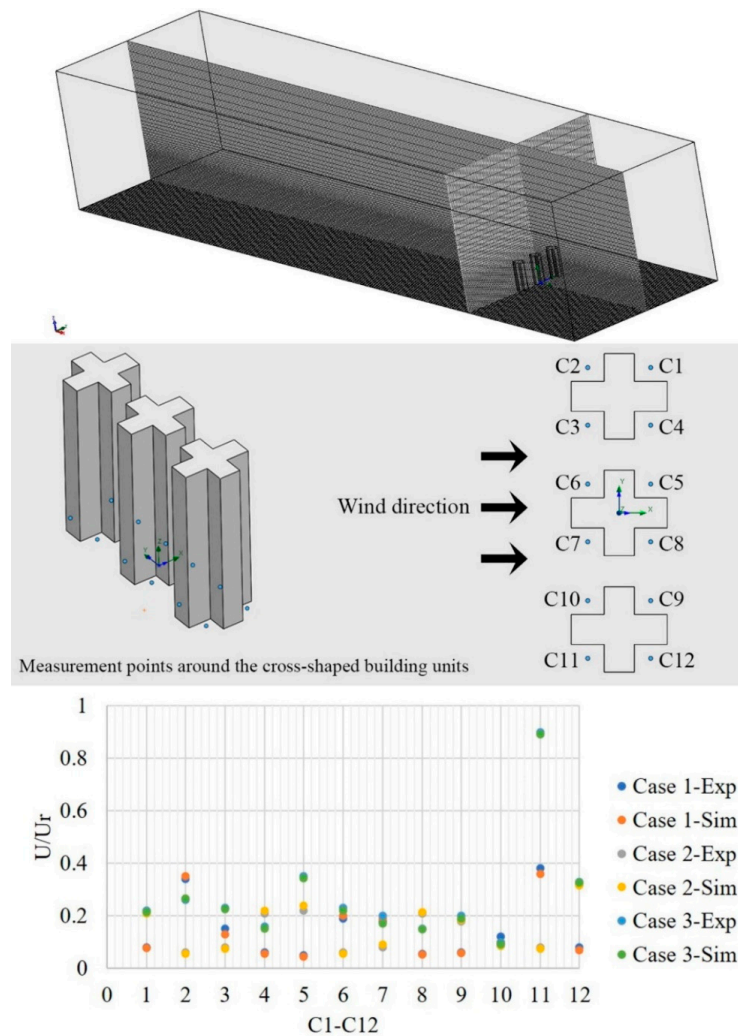


Figure 5. (Top): Meshing of the wind tunnel experiment for CFD simulation. (Middle): The configuration of the cross-shaped buildings and the measurement points around the building units. (Bottom): The U/U_r at C1-C12 of the experiment (Exp) and simulation (Sim).

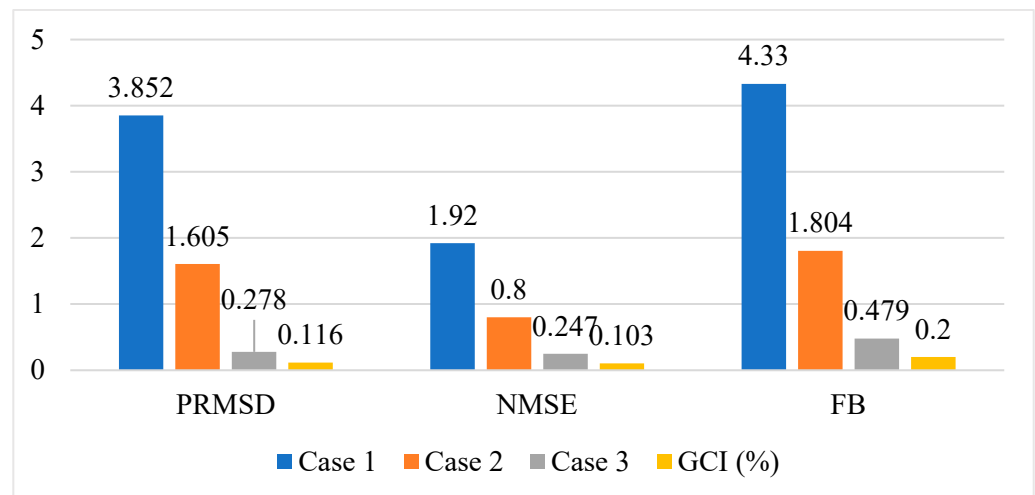


Figure 6. The statistical discrepancies of the U/U_r of the experiment and simulation.

In the equations above, n was the number of measurement points, E_i was an experimental value at a point, S_i was a CFD simulation value at a point, E_m was the mean experimental value, S_m was the mean CFD simulation value, $PRMSD_{ES}$, $NMSE_{ES}$, and FB_{ES} were the predicted root mean square division, normalized mean square error, and fractional bias between the experiment and simulation respectively.

2.7. Influence Evaluation

(1) Analysis of IAs

Lots of previous studies showed that wind velocity was a crucial factor in the evaluation of wind environments. There were former investigations of the pedestrian-level wind conditions using parameters related to wind velocities. The normalization of mean wind speed (U/U_r) was such utilization that could determine the wind speed statistics and the boundaries of low-velocity areas (LVAs) and high-velocity areas (HVAs) by combining specific wind conditions based on wind-velocity magnitudes [36]. The air-flow data were usually collected from certain points or lines around the buildings [22].

In our study, a novel method based on image processing of velocity magnitudes was proposed to quantitatively evaluate the Influenced Areas (IAs) with various velocities on the pedestrian-level plane. The utilization of IAs could evaluate the wind environments for large areas around buildings in a more comprehensive way, in comparison with certain points or lines. The IAs with various wind velocities were presented in the wind-velocity magnitudes by using various colors. The digital images of the magnitudes were formed by pixels that were the smallest units with separate colors for an intensity value. A computational image processing tool was used to calculate the IAs by calculating the pixel numbers of areas with different colors in the digital images of wind-velocity magnitudes [37]. Then, the actual influenced areas around the buildings could be obtained based on proportional conversions.

In this study, wind velocities on the pedestrian-level plane at the height of 1.5 m were considered as a key element of the evaluations. IAs with various wind velocities, LVAs, and HVAs in all the cases were evaluated quantitatively. The wind velocity of LVAs was in the range of 0.000–0.533 m/s (U/U_r : 0.0–0.3, the reference velocity = 1.33 m/s); the wind velocity of HVAs was in the range of 1.422–1.600 m/s (U/U_r : 1.0–1.2, the reference velocity = 1.33 m/s). The IAs with the velocity range of 1.244–1.422 m/s would not be presented because they were infinite, as the original velocity belonged to this range. Wind-velocity magnitudes on the vertical planes paralleled with the wind direction, air-pressure magnitudes, and wind-flow streamlines were together used to help in the analysis.

(2) Correlation and MLR analysis of influences from geometrical variables

The method aimed to analyze the influences on LVAs and HVAs of geometrical variables of T-form buildings, especially for different bulge-part sizes. The normality test was implemented first using the Shapiro-Wilk test (S-W test) before correlation and Multivariate Linear Regression (MLR) analysis [38]. Pearson Correlation Coefficients (PCCs) were calculated to show the strength of a linear relationship between the IAs and geometrical variables [39]. The linear correlation relationships between the independent and dependent variables were further analyzed and described using the MLR analysis [40]. More information on MLR quality could be obtained through the analysis of variance [41].

3. Results Analysis and Discussion

This section conducts a comprehensive analysis of the results pertaining to T-form buildings characterized by two typical heights and is divided into two parts. Utilizing the aforementioned methodology, we quantitatively compare the influences of their bulge parts on wind environments. This analysis encompasses comparisons across multiple parameters, including Influenced Areas (IAs), Low-Velocity Areas (LVAs), High-Velocity Areas (HVAs), air-pressure distributions, wind-flow streamlines, and statistical assessments. In the analysis of the results, the quantitative impacts of bulge-part sizes on wind environments have been meticulously examined, distinguishing between two distinct scenarios represented in Parts 1 and 2.

3.1. Part 1: 36 m-Height Buildings with Different Bulge-Part Lengths

Part 1 of the study delved into the impact of varying bulge-part lengths on wind environments surrounding T-form high-rise residential buildings, each standing at a height of 36 m (Figure 7). For comparative analysis, two cases featuring rectangular-form buildings were considered: Case 1 (10 m × 20 m × 36 m) and Case 5 (12 m × 20 m × 36 m). Notably, Case 1 exhibited the most pronounced influence on the wind environment, as indicated by its highest IA among all cases. Subsequently, as the bulge-part length increased from Case 2 (6 m) to Case 5, the IA progressively decreased, with Case 5 demonstrating the least influence (Figure 8). Furthermore, the LVA was observed to follow a similar trend: Case 1 boasted the longest LVA, gradually diminishing through Case 2, Case 3, and Case 4, culminating in the shortest LVA for Case 5. Similarly, the HVAs along the lateral sides exhibited a decreasing trend with increasing bulge-part length, with Case 1 featuring the largest HVAs and Case 5 showcasing the smallest areas (Figure 8). To synthesize, Part 1 findings reveal a diminishing impact on wind environments of T-form buildings as the bulge-part length increases.

In Part 1 of our investigation, we observed a correlation between the fluctuations in IAs at different wind velocities and alterations in air pressure and wind flow dynamics (Figure 9). Typically, the bulge parts of the structures were situated on the windward side, aligning with prevalent seasonal wind directions, notably during summer and transitional seasons. Consequently, incoming winds encountered these bulge parts initially upon approaching the buildings. Across the spectrum from Case 1 to Case 5, it was noted that the low-pressure regions behind the buildings and the high-pressure zones ahead of them diminished with the increase in bulge-part length. Concurrently, the vortices on the leeward sides of the structures decreased both in size and frequency as the length extended. These observations were consistent with the patterns discerned in the IAs across varied wind velocities, as detailed earlier.

In summary, we focused on comparatively shorter high-rise residential T-form buildings in Part 1, standing at a height of 36 m, characterized by relatively modest bulge-part dimensions. These buildings exemplify the typical 12-floor structures, featuring two apartments per floor, with correspondingly smaller bulge parts spanning 6 to 10 m. Through the comparison of five cases with varying bulge-part lengths, we observed a consistent decrease in IAs, HVAs, and LVAs as the bulge-part length increased.

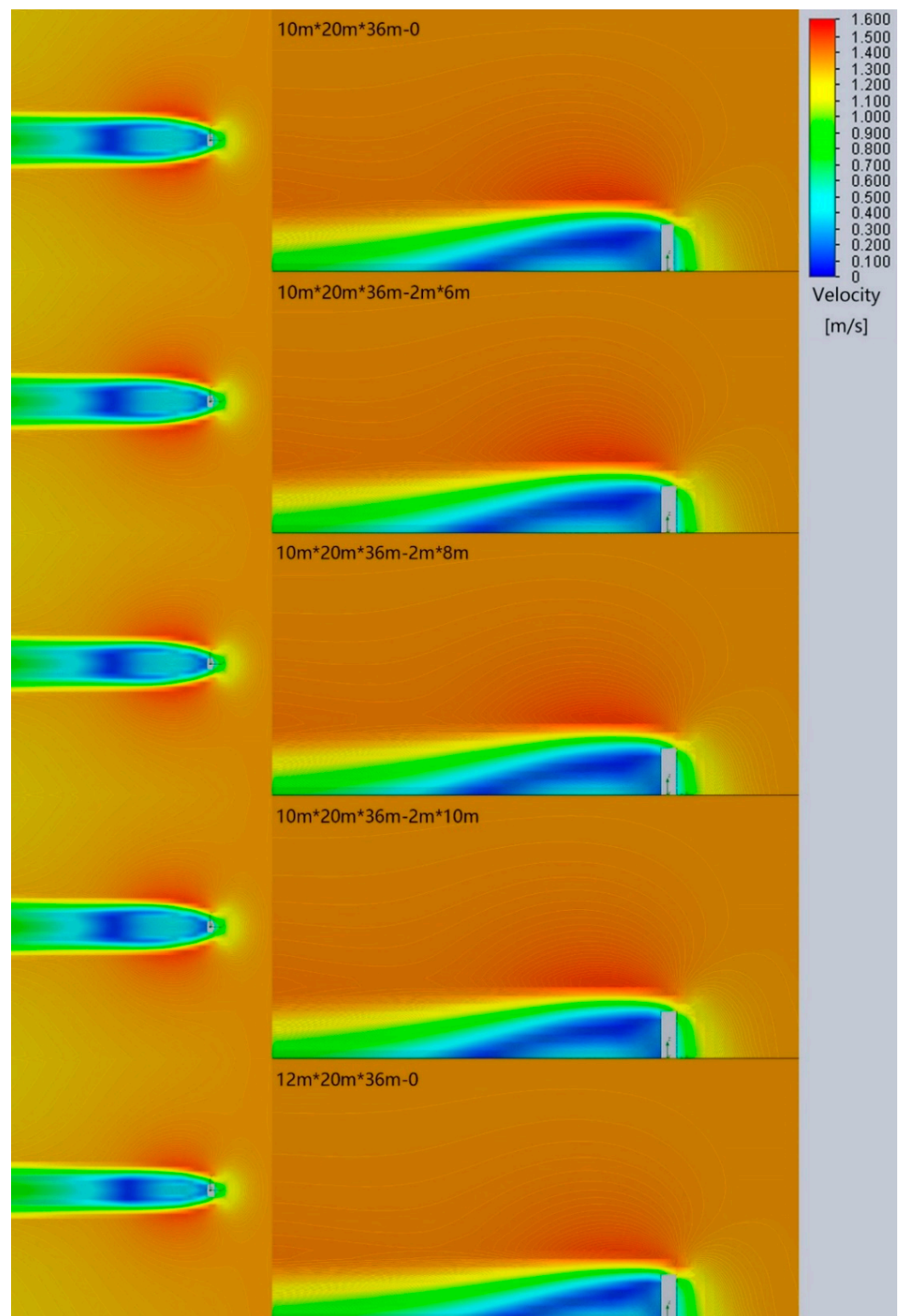


Figure 7. Comparisons of wind-velocity magnitudes on horizontal and vertical planes of Case 1–Case 5 of Part 1.

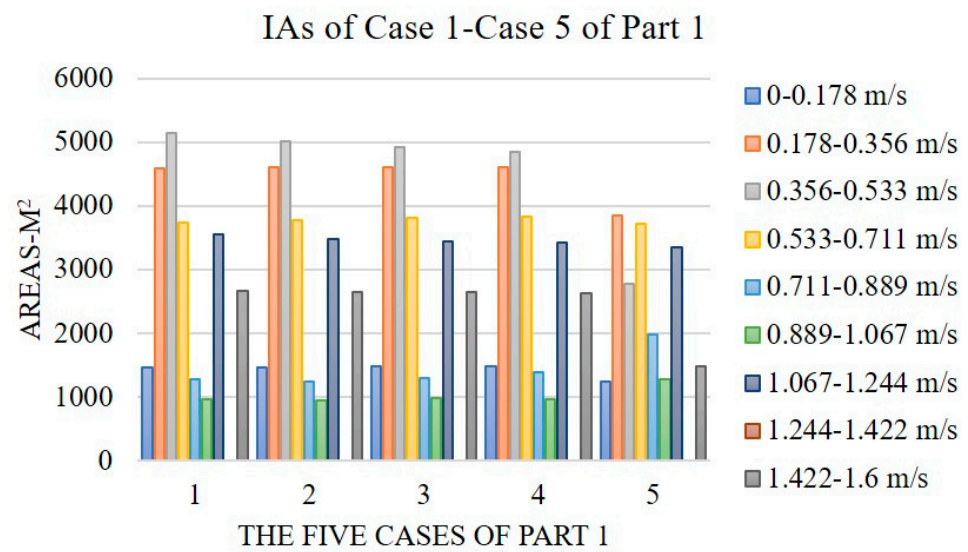


Figure 8. The IAs with different wind velocities of Part 1.

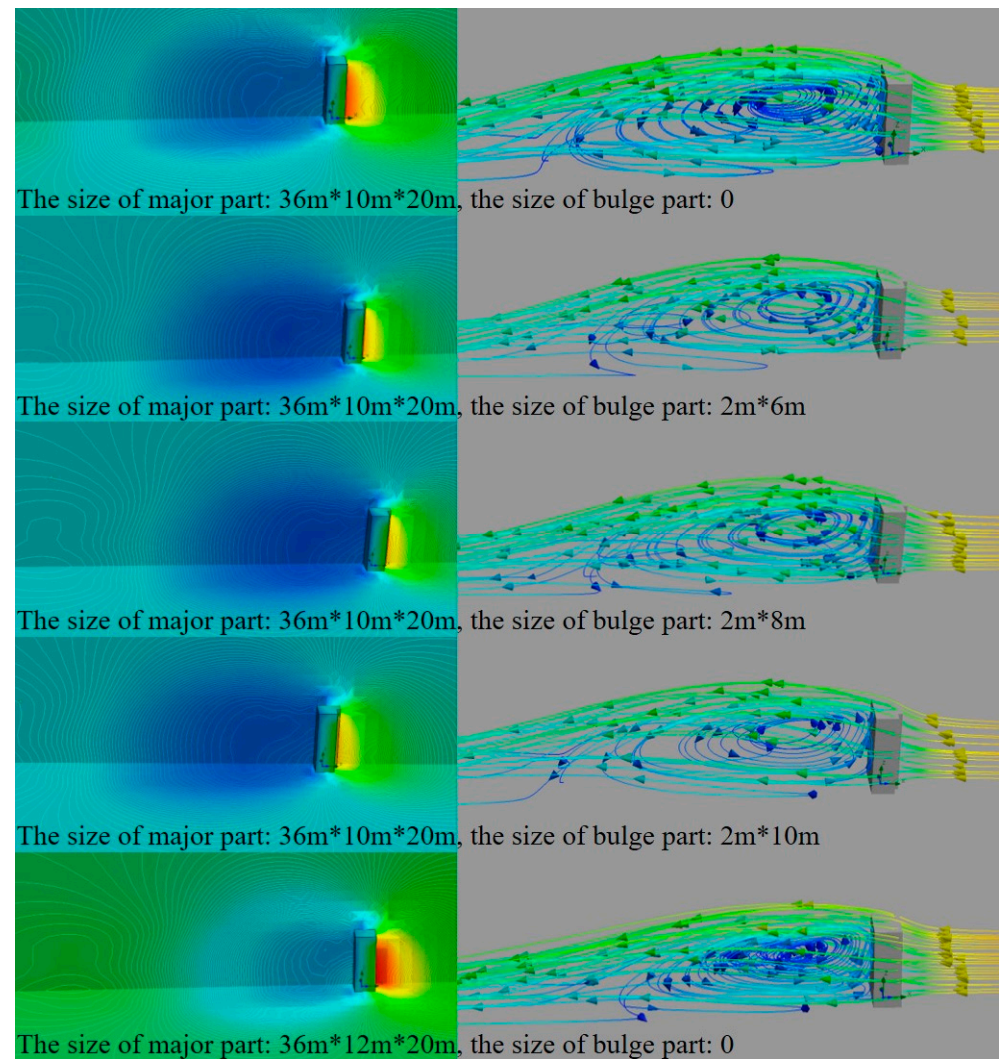
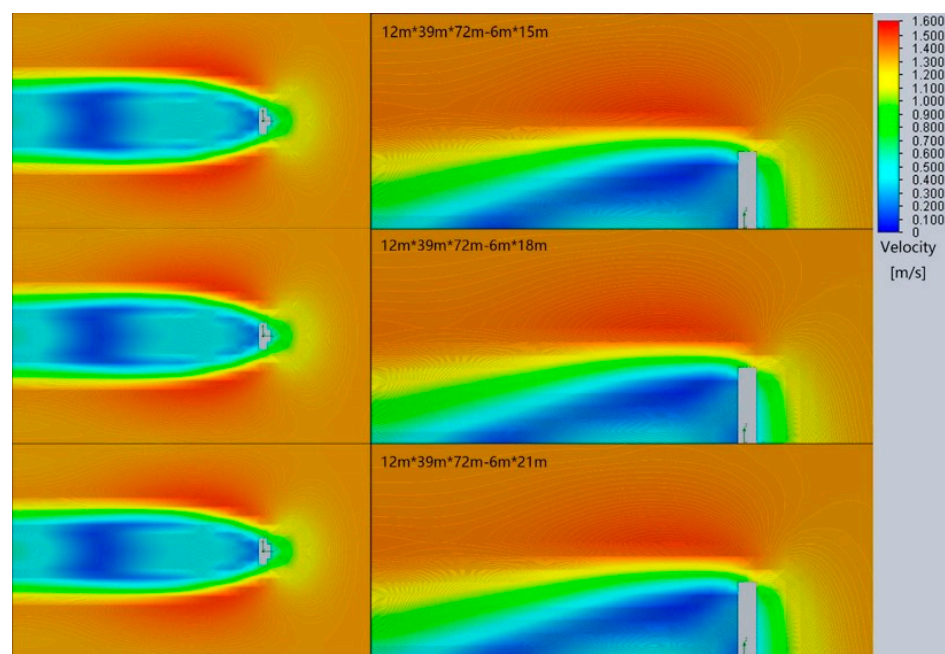


Figure 9. The comparisons of wind-flow streamlines (right) and air-pressure magnitudes (left) on the horizontal, vertical planes and building surfaces of Part 1.

3.2. Part 2: 72 m-Height Buildings with Different Bulge-Part Lengths and Widths

Part 2 of our study delved into the impact of varying lengths and widths of bulge parts on wind environments surrounding high-rise residential T-form buildings towering at a height of 72 m. In Case 1, characterized by a bulge-part length of 15 m and a width of 6 m, we observed the most significant IA on the wind environment. Conversely, Case 3, with a bulge-part length of 21 m and the same width, exhibited the least IA, with Case 2 falling in between these extremes (Figure 10). Correspondingly, Case 1 boasted the largest LVA, gradually decreasing through Case 2 and culminating in the smallest LVA in Case 3 (Figure 10). Similarly, the HVAs on the lateral sides followed a diminishing trend from Case 1 to Case 3. Notably, similar trends were observed in Case 4, Case 5, and Case 6, where the bulge-part width was fixed at 12 m, as well as in Case 7, Case 8, and Case 9, where the width expanded to 18 m (refer to Figures 10–12). Overall, our findings indicate a consistent reduction in the influences on wind environments of T-form buildings as the bulge-part lengths increased in Part 2.



IAs of Case 1-Case 3 of Part 2

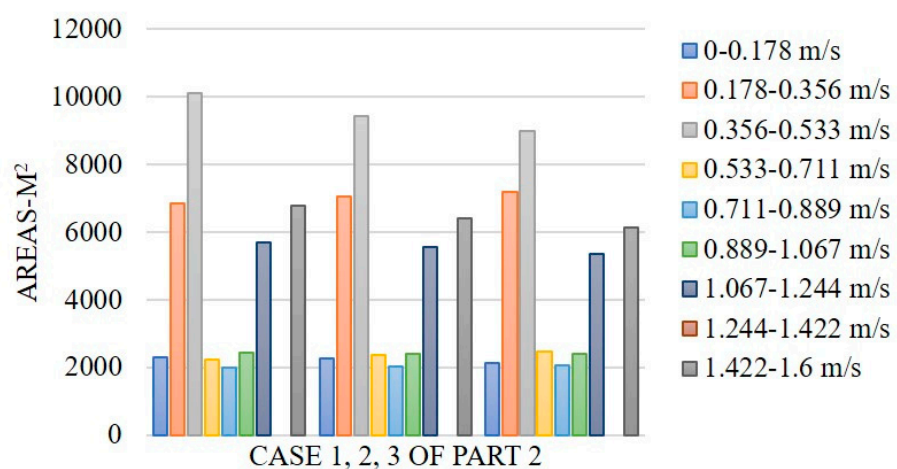
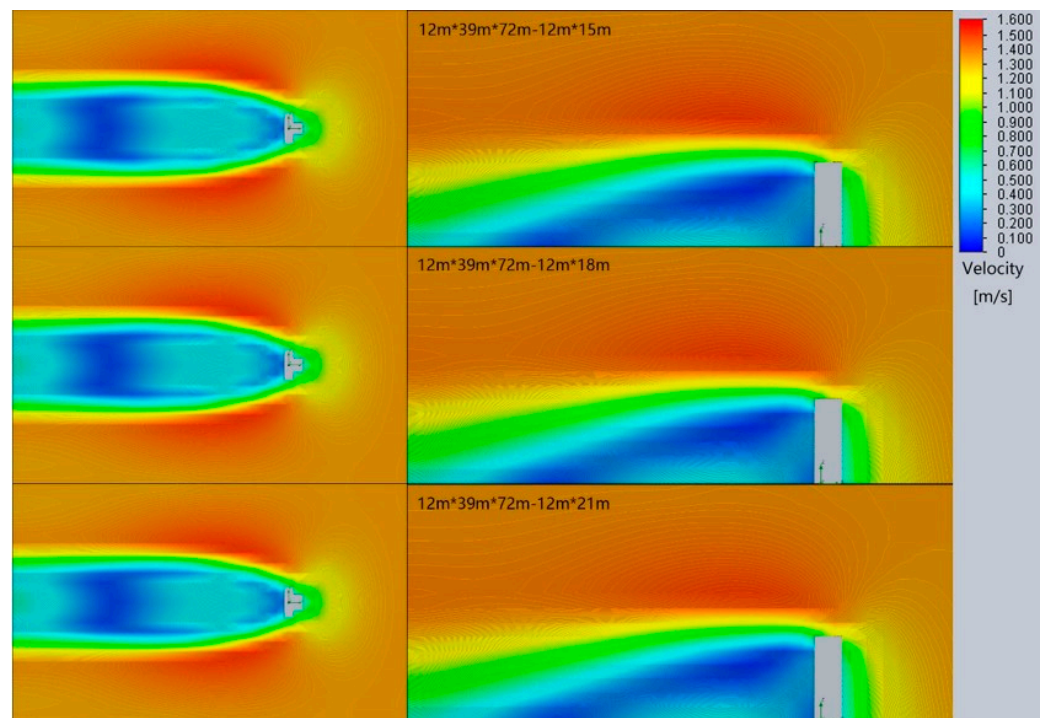


Figure 10. Top: Wind-velocity magnitudes on horizontal and vertical planes of Case 1–Case 3 of Part 2. Bottom: The IAs with different velocities of Case 1–Case 3 of Part 2.



IAs of Case 4–Case 6 of Part 2

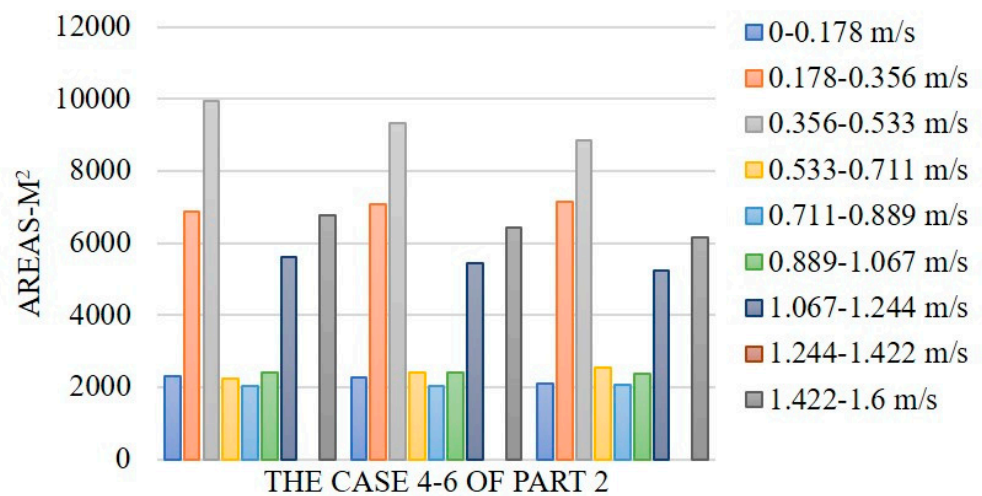
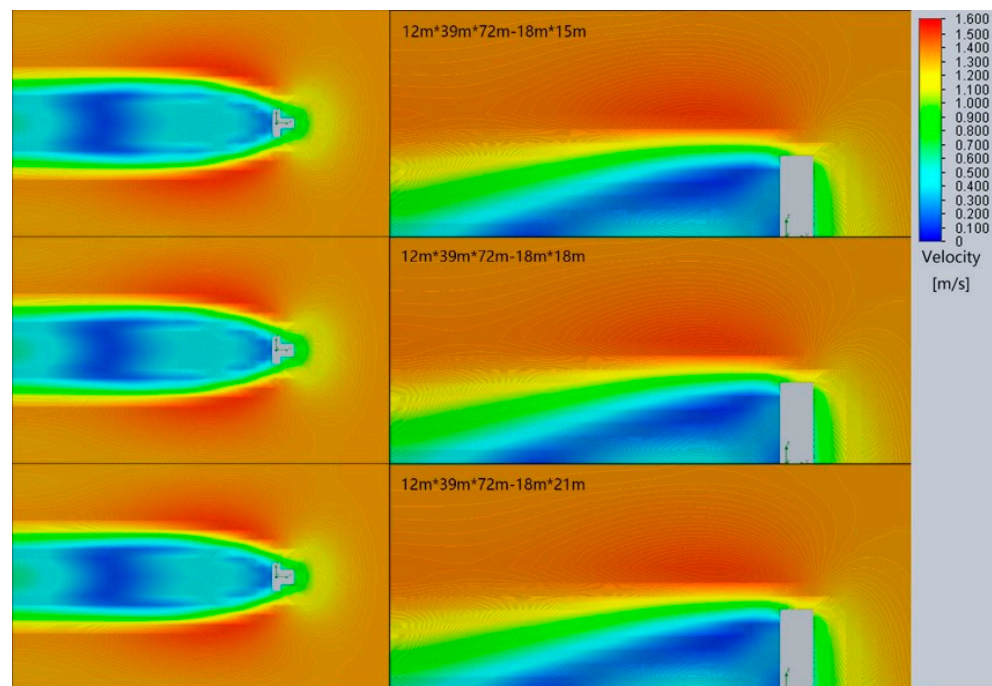


Figure 11. (Top): Wind-velocity magnitudes on horizontal and vertical planes of Case 4–Case 6 of Part 2. (Bottom): The IAs with different velocities of Case 4–Case 6 of Part 2.

Additionally, we examined buildings with different bulge-part widths (6 m, 12 m, and 18 m) for comparative analysis (Figures 10–12). When the bulge-part length remained constant, structures with a width of 6 m exhibited the largest IA, while those with an 18 m width displayed the least IA. Buildings with a 12 m width fell between these extremes. Furthermore, as the width increased, both LVAs and HVAs demonstrated a decreasing trend. Although differences among the cases were marginal, the reductions in IAs were discernible. In summary, our study highlights a decrease in the influences on wind environments of T-form buildings with the expansion of bulge-part widths in Part 2.

In a manner reminiscent of Part 1, we observed in Part 2 that the fluctuations in Influence Areas (IAs) across different wind velocities corresponded to shifts in air pressure and wind flow dynamics across all nine cases (Figure 13). Winds encountered the bulge parts on the windward sides upon approaching the buildings. Taking Cases 1 through 3 as an illustration, we noted a reduction in both the low-air-pressure areas on the leeward

sides and the high-air-pressure areas on the windward sides as the bulge-part length increased from Case 1 to Case 3. Simultaneously, the vortices generated on the leeward sides diminished in size and intensity with the elongation of the bulge-part length. This trend closely mirrored that observed in Cases 4 through 6 and Cases 7 through 9, as revealed by simulation results (Figure 13). The results were further analyzed to discern the impacts of bulge-part widths. Notably, as the width increased, both the low-air-pressure and high-air-pressure areas diminished, and the vortices decreased in size and intensity. In summary, the discrepancies in air pressure between the windward and leeward sides of the buildings decreased with the elongation and widening of the bulge parts. Larger bulge parts facilitated smoother wind flow around the T-form buildings. These observations elucidate how increasing the length and width of the bulge parts correlates with a decrease in total IAs across various wind velocities.



IAs of Case 7-Case 9 of Part 2

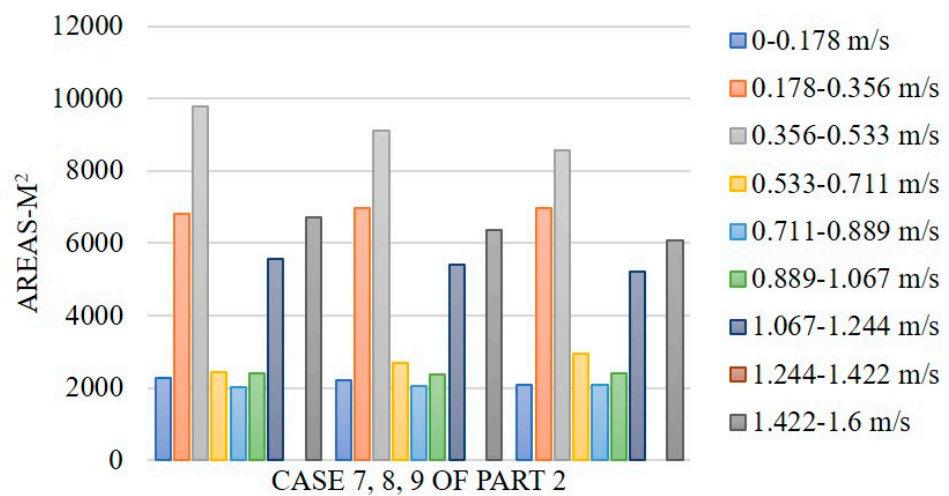


Figure 12. (Top): Wind-velocity magnitudes on horizontal and vertical planes of Case 7–Case 9 of Part 2. (Bottom): The IAs with different velocities of Case 7–9 of Part 2.

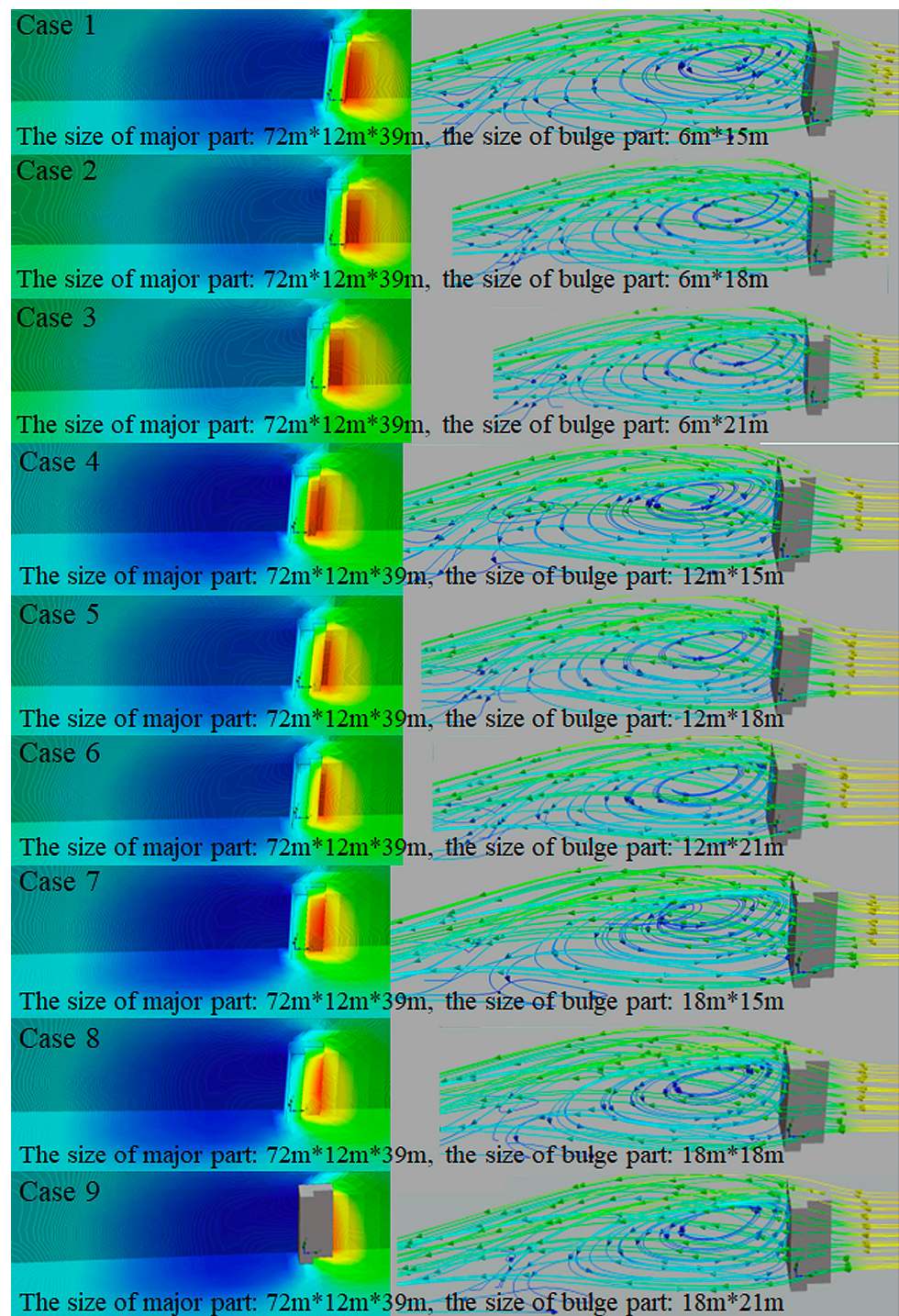


Figure 13. (Left): Comparison of air-pressure magnitudes on horizontal and vertical planes and building surfaces of Part 2. (Right): Comparison of wind-flow streamlines of Part 2.

In Part 2, our attention shifted to taller buildings, which reached a height of 72 m and were equipped with larger bulge parts. These structures represent the archetype of 24-floor buildings, accommodating four apartments per floor and boasting relatively expansive bulge parts ranging from 15 to 21 m in length and 6 to 18 m in width. Through a quantitative comparison of nine cases encompassing diverse combinations of bulge-part lengths and widths, we consistently observed a reduction in IAs, HVAs, and LVAs as both the lengths and widths of the bulge-parts increased. Notably, our analysis unveiled that the effects of length extensions slightly outweighed those of width expansions, leading to more

pronounced reductions in HVAs and LVAs with increases in length. In summary, our comprehensive analysis underscores the critical role of bulge-part dimensions in shaping wind environments around T-form buildings, with the elongation of lengths notably influencing reductions in influenced areas with different wind velocities, particularly HVAs and LVAs.

The analyses of Part 1 and Part 2 reveal that alterations in the IAs, HVAs, and LVAs of both Part 1 and Part 2 correlate significantly with reductions in low-pressure zones, high-pressure zones, and vortices on the leeward sides. Specifically, enlarging the dimensions of the bulging sections leads to a decrease in IAs, LVAs, and HVAs, along with reductions in low and high-pressure areas and diminished vortex sizes on the leeward side of the structures. Conversely, diminishing the dimensions of the bulge parts yields contrasting effects. Examination of wind-flow streamlines indicates that the bulge sections serve to bifurcate winds and redirect them around the building. Consequently, enhancing the lengths and widths of the bulge sections promotes outdoor ventilation. Notably, increasing the length of the bulge section tends to have a slightly more pronounced effect on ventilation promotion compared to increasing its width. Expanding the dimensions of the bulge sections encourages airflow around T-form buildings. These findings offer valuable insights for formulating design strategies aimed at enhancing wind conditions surrounding high-rise residential T-form buildings.

3.3. Comparison of Influences on LVAs and HVAs from Geometrical Variables

The statistical analysis revealed that all geometrical variables, including LVAs and HVAs, exhibited non-normal distributions. Figure 14 illustrates a correlation-strength heat map depicting the influences of wind environments and geometrical variables of T-form buildings. Examination of PCCs yielded several significant findings: (1) The PCC between H and LVA, as well as between H and HVA, both stood at 0.98, mirroring the correlation strength between LM and LVA, and LM and HVA, all four of which were the highest among the correlations observed. (2) The PCC between WM and LVA was 0.73, with a slightly higher PCC of 0.76 observed between WM and HVA. (3) Regarding the bulge part, the PCC between LB and LVA, as well as between LB and HVA, reached 0.88, indicating a strong correlation akin to that observed between the major part dimensions and influenced areas with different wind velocities. The correlation analysis inferred the following insights: (1) The height and length of the primary section of T-form buildings exerted the most significant influence on both LVA and HVA. (2) The width of the primary section exhibited a stronger impact on HVA compared to LVA. (3) The size of the bulge part demonstrated a notable influence on both LVA and HVA, aligning closely with the dimensions of the primary section.

The MLR analysis unveiled robust linear correlations between various geometrical variables. For instance, the strongest linear correlations were observed between the Lengths of LVA and LM (p value = 7.70×10^{-9}), as well as between LVA and WM (p value = 3.02×10^{-6}). The analysis of variance underscored the significant influence of both LM (p value = 3.039×10^{-12}) and WM (p value = 5.241×10^{-6}) on the linear model. Similarly, examining the bulge-part dimensions, a notable linear correlation surfaced between LVA and LB (p value = 0.005954), contrasting with the comparatively weaker correlation between LVA and WB (p value = 0.09636). Moreover, the analysis of variance indicated the relatively pronounced influence of LB on the linear model (p value = 0.005954).

Furthermore, the MLR analysis highlighted robust linear correlations between HVA and both LM (p value = 8.94×10^{-8}) and WM (p value = 0.000107). Notably, LM (p value = 1.965×10^{-11}) and WM (p value = 0.0002716) demonstrated substantial influence on the linear model, as indicated by the analysis of variance. However, regarding the bulge-part dimensions, the linear correlation between HVA and LB (p value = 0.0130848) was comparatively weaker than that observed between LVA and LB, while the correlation between HVA and WB exhibited even less strength (p value = 0.9065749).

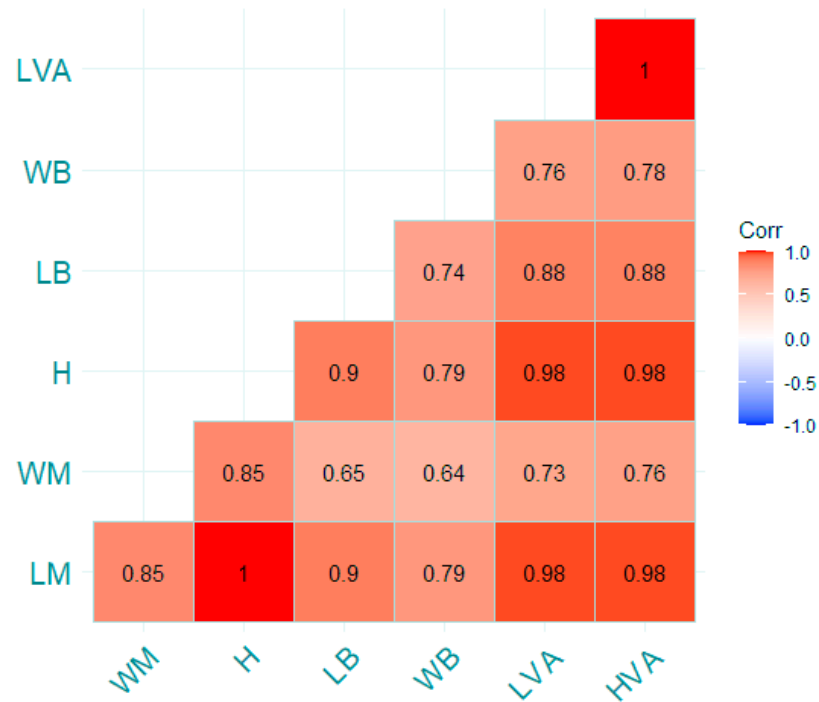


Figure 14. The correlation-strength (Pearson Correlation) heat map of the influences on wind environments and geometrical variables of T-form buildings.

In Figure 15, the multivariate regression models were graphically represented, with a thorough examination of the residuals versus fitted plots revealing numerous nonlinear patterns. However, the normal Quantile-Quantile (Q-Q) plot suggested that the residuals adhered to a straight dashed line, indicative of a normal distribution.

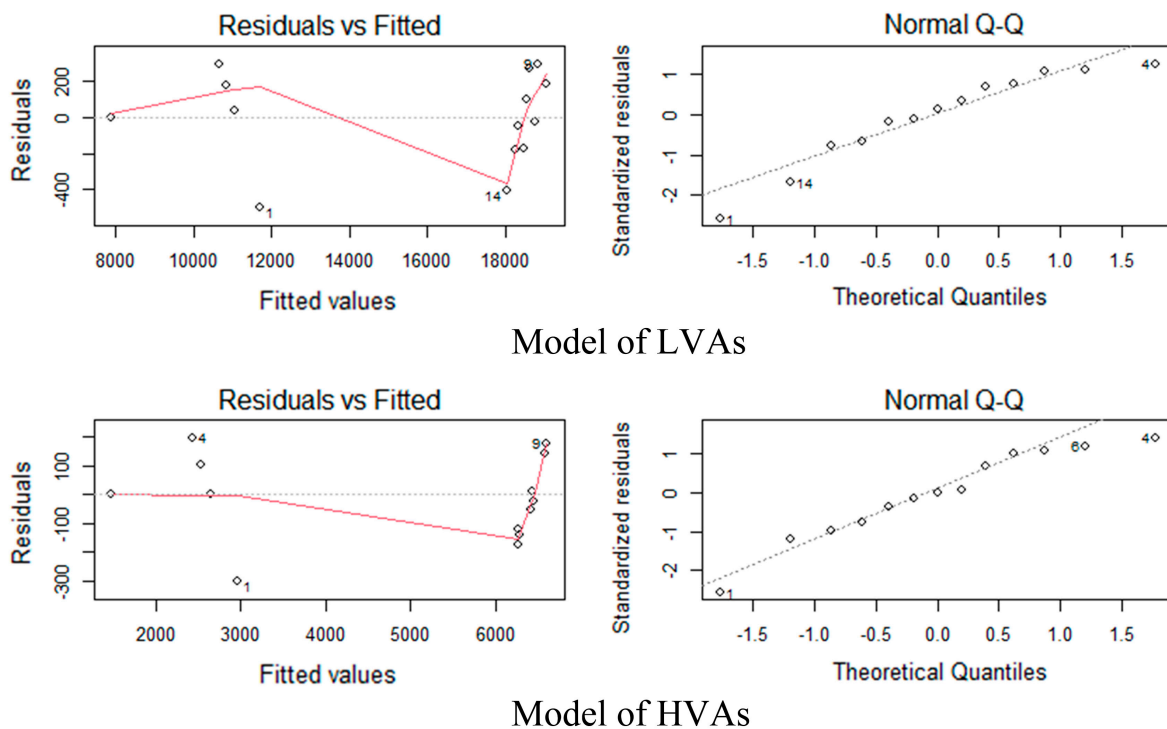


Figure 15. Visualization of the multivariate regression models. (Top): the model of LVAs; (bottom): the model of HVAs.

3.4. Research Limitations and Future Research

Regarding limitations, it is important to note that this study exclusively delved into the wind dynamics surrounding high-rise residential T-form buildings in isolation without considering the presence of neighboring structures. Furthermore, the investigation focused solely on the effects of bulge-part sizes and typical architectural variables within specified ranges. It's worth acknowledging that other variables pertaining to building geometries or configurations could potentially exert diverse influences on wind patterns. Additionally, the scope of our study encompassed a relatively restricted number of cases, and expanding the sample size could potentially provide a more precise depiction of prevailing trends.

Future studies should delve into the impact of neighboring structures on wind patterns around T-form high-rises, exploring factors like height and configuration for insights into urban airflow dynamics. Investigating beyond bulge-part sizes to include variables such as setbacks and facade articulations can enhance understanding of their combined influence on wind environments. Expanding the sample size to include diverse building configurations, site conditions, and geographic locations will improve generalizability and offer insights into various urban contexts. Adopting a holistic approach that integrates factors like thermal comfort, air quality, and pedestrian experience can lead to more comprehensive design solutions. Continual validation and refinement of computational models used for simulating wind environments are crucial for improving accuracy and reliability. Additionally, conducting post-occupancy evaluations and long-term monitoring of T-form buildings can provide valuable feedback on design effectiveness and occupant satisfaction, guiding iterative improvements.

4. Conclusions

This paper presents a comprehensive investigation focusing on the quantitative assessment of wind environment influences surrounding high-rise residential T-form buildings, specifically examining the effects of varying bulge-part geometries. The study systematically evaluates the impact of different bulge-part sizes on wind environments surrounding typical T-form high-rise residential structures with common heights, considering buildings of 36 m and 72 m in height. The bulge parts, situated on the windward side with vertical windward surfaces, are analyzed using a methodology integrating parametric modeling, CFD, and IAs analysis. Efficient parametric modeling algorithms facilitate the creation of T-form building models, while CFD simulations based on the RANS method, validated through wind tunnel experiments, enable the quantitative comparison of various building scenarios. The study contributes original insights to wind environment research pertaining to contemporary high-rise residential T-form buildings, offering a novel quantitative comparison of wind environment influences based on IAs calculations within different velocity ranges. This research provides valuable information for the development of sustainable architectural design strategies aimed at optimizing outdoor wind environments for high-rise residential communities and urban microclimates. Specific findings can be summarized as follows.

- (1) The influences on wind environments decrease as the bulge-part sizes increase; the decrease of the bulge-part sizes can cause a contrary effect. The study reveals that increasing bulge-part sizes lead to decreased influences on wind environments, with changes in IAs, LVAs, and HVAs correlating with variations in air pressure and vortices. Both length and width extensions of bulge parts contribute to reducing wind environment influences, thereby promoting outdoor ventilation around T-form buildings.
- (2) Our quantitative comparison indicates that the promotion of outdoor ventilation caused by the increase of the bulge-part length is more than the increase of the bulge-part width for a T-form building. Quantitative comparisons demonstrate that increasing bulge-part length yields greater promotion of outdoor ventilation compared to width extensions for T-form buildings. The analysis highlights a notable decrease in LVAs on the leeward side with elongation of the bulging part, indicating enhanced airflow circulation around windward corners.

- (3) It is recommended to design the T-form buildings with relatively large bulge parts on the windward side for enhancing outdoor ventilation. Recommendations suggest designing T-form buildings with relatively large bulge parts on the windward side to enhance outdoor ventilation. Prioritizing length extensions over width increases is advised, as longer bulge parts demonstrate more significant effects in promoting outdoor ventilation and avoiding potential sunlight blockage associated with wider bulge parts.

Overall, this research underscores the importance of bulge-part geometries in shaping wind environments around high-rise residential T-form buildings, offering actionable insights for architects and urban planners seeking to optimize outdoor ventilation and improve urban microclimates.

Author Contributions: Conceptualization, H.G. and Y.H.; methodology, Y.H.; software, Y.L.; validation, H.G., Y.L. and Y.H.; formal analysis, H.G. and Y.H.; investigation, Y.L.; resources, Y.H.; data curation, Y.L.; writing—original draft preparation, H.G., Y.L. and Y.H.; writing—review and editing, Y.H.; visualization, H.G., Y.L. and Y.H.; supervision, Y.H.; project administration, H.G.; funding acquisition, H.G., Y.L. and Y.H. All authors have read and agreed to the published version of the manuscript.

Funding: This research was supported by the Natural Science Foundation of China (NSFC Grant No. 42371471) and the Open Fund of Key Laboratory of Urban Land Resources Monitoring and Simulation, Ministry of Natural Resources of China (Grant No. KF-2022-07-022; No. KF-2022-07-002).

Institutional Review Board Statement: Not applicable.

Informed Consent Statement: Not applicable.

Data Availability Statement: The original contributions presented in the study have been included in the article.

Conflicts of Interest: The authors declare no conflicts of interest. The funders had no role in the design of the study; in the collection, analyses, or interpretation of data; in the writing of the manuscript; or in the decision to publish the results.

References

1. Angel, S.; Sheppard, S.C.; Civco, D.L. *The Dynamics of Global Urban Expansion*. Transport and Urban Development Department; The World Bank: Washington, DC, USA, 2005.
2. United Nations. *World Urbanization Prospects: The 2014 Revision*; United Nations: New York, NY, USA, 2014.
3. Zhou, C.; Wang, Z.; Chen, Q.; Jiang, Y.; Pei, J. Design optimization and field demonstration of natural ventilation for high-rise residential buildings. *Energy Build.* **2014**, *82*, 457–465. [[CrossRef](#)]
4. United Nations. *Transforming Our World: The 2030 Agenda for Sustainable Development*; United Nations: New York, NY, USA, 2015.
5. Blocken, B.; Carmeliet, J. Pedestrian wind environment around buildings: Literature review and practical examples. *J. Therm. Envel. Build. Sci.* **2003**, *28*, 1097–1963. [[CrossRef](#)]
6. Stathopoulos, T. Pedestrian level winds and outdoor human comfort. *J. Wind. Eng. Ind. Aerodyn.* **2006**, *94*, 769–780. [[CrossRef](#)]
7. Blocken, B.; Janssen, W.D.; Hooff, T.V. CFD simulation for pedestrian wind comfort and wind safety in urban areas: General decision framework and case study for the Eindhoven University campus. *Environ. Model. Softw.* **2012**, *30*, 15–34. [[CrossRef](#)]
8. Stathopoulos, T.; Baskaran, B.A. Computer Simulation of Wind Environmental Conditions around Buildings. *Eng. Struct.* **1996**, *18*, 876–885. [[CrossRef](#)]
9. Tsang, C.W.; Kwok, K.C.S.; Hitchcock, P.A. Wind tunnel study of pedestrian level wind environment around tall buildings: Effects of building dimensions, separation and podium. *Build. Environ.* **2012**, *49*, 167–181. [[CrossRef](#)]
10. Luo, W.; Dong, Z.; Qian, G.; Lu, J. Wind tunnel simulation of the three-dimensional airflow patterns behind cuboid obstacles at different angles of wind incidence, and their significance for the formation of sand shadows. *Geomorphology* **2012**, *139*, 258–270. [[CrossRef](#)]
11. Du, Y.X.; Mak, C.M.; Tang, B.S. Effects of building height and porosity on pedestrian level wind comfort in a high-density urban built environment. *Build. Simul.* **2018**, *11*, 1215–1228. [[CrossRef](#)]
12. Jiang, Z.; Gao, W.; Yao, W. Research on the wind environment in an enclosed courtyard: Effect of the opening position, size and wind angle. *Urban Clim.* **2023**, *52*, 101737. [[CrossRef](#)]
13. Jie, P.; Su, M.; Gao, N.; Ye, Y.; Kuang, X.; Chen, J.; Li, P.; Grunewald, J.; Xie, X.; Shi, X. Impact of urban wind environment on urban building energy: A review of mechanisms and modeling. *Build. Environ.* **2023**, *245*, 110947. [[CrossRef](#)]
14. Oh, G.; Yang, M.; Choi, J.-I. Large-eddy simulation-based wind and thermal comfort assessment in urban environments. *J. Wind. Eng. Ind. Aerodyn.* **2024**, *246*, 105682. [[CrossRef](#)]

15. Ying, X.; Qin, X.; Shen, L.; Yu, C.; Zhang, J. An intelligent planning method to optimize high-density residential layouts considering the influence of wind environments. *Heliyon* **2023**, *9*, e13051. [[CrossRef](#)] [[PubMed](#)]
16. Chen, L.; Mak, C.M.; Hang, J.; Dai, Y.; Niu, J.; Tse, K.T. Large eddy simulation study on pedestrian-level wind environments around elevated walkways and influential factors in ideal urban street canyons. *Build. Environ.* **2023**, *235*, 110236. [[CrossRef](#)]
17. Liu, J.; Niu, J. CFD simulation of the wind environment around an isolated high-rise building: An evaluation of SRANS, LES and DES models. *Build. Environ.* **2016**, *96*, 91–106. [[CrossRef](#)]
18. Zhu, C.L.; Wei, H.Y.; Long, H. *Design Theories of Residential Architecture*; China Architecture & Building Press: Beijing, China, 2011.
19. Iqbal, Q.M.Z.; Chan, A.L.S. Pedestrian level wind environment assessment around group of high-rise cross-shaped buildings: Effect of building shape, separation and orientation. *Build. Environ.* **2016**, *101*, 45–63. [[CrossRef](#)]
20. Franke, J.; Hellsten, A.; Schlünzen, H.; Carissimo, B. *Best Practice Guideline for the CFD Simulation of Flows in the Urban Environment*; COST Office: Hamburg, Germany, 2007.
21. He, Y.; Schnabel, M.A.; Mei, Y. A novel methodology for architectural wind environment study by integrating CFD simulation, multiple parametric tools and evaluation criteria. *Build. Simul.* **2019**, *13*, 609–625. [[CrossRef](#)]
22. Li, Y.; Chen, L. Study on the influence of voids on high-rise building on the wind environment. *Build. Simul.* **2019**, *13*, 419–438. [[CrossRef](#)] [[PubMed](#)]
23. Aynsley, R.M. Politics of pedestrian level urban wind control. *Build. Environ.* **1989**, *24*, 291–295. [[CrossRef](#)]
24. Sobachkin, A.; Dumnov, G. Numerical Basis of CAD-Embedded CFD. In Proceedings of the NAFEMS World Congress, Salzburg, Austria, 28–30 May 2014.
25. Lam CK, G.; Bremhorst, K. A modified form of the k- ϵ model for predicting wall turbulence. *J. Fluids Eng.* **1981**, *103*, 456. [[CrossRef](#)]
26. Launder, B.E.; Spalding, D.B. The numerical computation of turbulent flows. *Comput. Methods Appl. Mech. Eng.* **1974**, *3*, 269–289. [[CrossRef](#)]
27. Richards, P.J.; Hoxey, R.P. Appropriate boundary conditions for computational wind engineering models using the k- ϵ turbulence model. *J. Wind. Eng. Ind. Aerodyn.* **1993**, *46*, 145–153. [[CrossRef](#)]
28. Wieringa, J. Updating the Davenport roughness classification. *J. Wind. Eng. Ind. Aerodyn.* **1992**, *41*, 357–368. [[CrossRef](#)]
29. Hang, J.; Li, Y. Age of air and air exchange efficiency in high-rise urban areas and its link to pollutant dilution. *Atmos. Environ.* **2011**, *45*, 5572–5585. [[CrossRef](#)]
30. Richardson, L.F. The approximate arithmetical solution by finite differences of physical problems involving differential equations, with an application to the stresses in a masonry dam. *R. Soc.* **1911**, *210*, 307–357.
31. Roache, P.J. Perspective: A method for uniform reporting of grid refinement studies. *J. Fluids Eng.* **1994**, *116*, 405–413. [[CrossRef](#)]
32. Vinchurkar, S.; Longest, P.W. Evaluation of hexahedral, prismatic and hybrid mesh styles for simulating respiratory aerosol dynamics. *Comput. Fluids* **2008**, *37*, 317–331. [[CrossRef](#)]
33. Wilks, D. *Statistical Methods in the Atmospheric Sciences*, 2nd ed.; Academic Press: Cambridge, MA, USA, 2006.
34. Chang, J.C.; Hanna, S.R. Air quality model performance evaluation. *Meteorol. Atmos. Phys.* **2004**, *87*, 167–196. [[CrossRef](#)]
35. Efthimiou, G.; Sabatino, J.; Martilli, A. Cost 732 in practice: The MUST model evaluation exercise. *Int. J. Environ. Pollut.* **2011**, *44*, 403.
36. Blocken, B.; Stathopoulos, T. CFD simulation of pedestrian-level wind conditions around buildings: Past achievements and prospects. *J. Wind. Eng. Ind. Aerodyn.* **2013**, *121*, 138–145. [[CrossRef](#)]
37. Schneider, C.A.; Rasband, W.S.; Eliceiri, K.W. NIH Image to ImageJ: 25 years of image analysis. *Nat. Methods* **2012**, *9*, 671–675. [[CrossRef](#)]
38. Liang, J.; Tang, M.-L.; Chan, P.S. A generalized Shapiro–Wilk W statistic for testing high-dimensional normality. *Comput. Stat. Data Anal.* **2009**, *53*, 3883–3891. [[CrossRef](#)]
39. DeLong, E.R.; DeLong, D.M.; Clarke-Pearson, D.L. Comparing the areas under two or more correlated receiver operating characteristic curves: A nonparametric approach. *Biometrics* **1988**, *44*, 837. [[CrossRef](#)]
40. Park, S.K.; Moon, H.J.; Min, K.C.; Hwang, C.; Kim, S. Application of a multiple linear regression and an artificial neural network model for the heating performance analysis and hourly prediction of a large-scale ground source heat pump system. *Energy Build.* **2018**, *165*, 206–215. [[CrossRef](#)]
41. Muddu, R.D.; Gowda, D.; Robinson, A.J.; Byrne, A. Optimisation of retrofit wall insulation: An Irish case study. *Energy Build.* **2021**, *235*, 110720. [[CrossRef](#)]

Disclaimer/Publisher’s Note: The statements, opinions and data contained in all publications are solely those of the individual author(s) and contributor(s) and not of MDPI and/or the editor(s). MDPI and/or the editor(s) disclaim responsibility for any injury to people or property resulting from any ideas, methods, instructions or products referred to in the content.